

Shoaling of Finite-Amplitude Rogue Waves

Saulo Mendes ^{1,2,3,*} Yuchen He,^{4,5} Jérôme Kasparian ^{2,3,†} and Amin Chabchoub ^{6,7,8,‡}

¹*University of Michigan–Shanghai Jiao Tong University Joint Institute,
Shanghai Jiao Tong University, Shanghai 200240, China*

²*Group of Applied Physics, University of Geneva,*

Rue de l'École de Médecine 20, 1205 Geneva, Switzerland

³*Institute for Environmental Sciences, University of Geneva,
Boulevard Carl-Vogt 66, 1205 Geneva, Switzerland*

⁴*Department of Civil and Environmental Engineering,
The Hong Kong Polytechnic University, Hong Kong SAR*

⁵*Department of Ocean Science and Engineering, Southern University of Science and Technology, Shenzhen 518055, China*

⁶*Marine Physics and Engineering Unit, Okinawa Institute of Science and Technology, Onna-son, Okinawa 904-0495, Japan*

⁷*Graduate School of Frontier Sciences, The University of Tokyo, Kashiwa, Chiba 277-8563, Japan*

⁸*Department of Infrastructure Engineering, The University of Melbourne, Parkville, Victoria 3010, Australia*

Rogue wave formation and enhancement over coastal areas have been documented over the last decade. However, this recent knowledge is in apparent contradiction with the established observation of sub-Gaussian wave statistics near shallow water. Current theories and experiments describe the rogue wave amplification near shallow water regimes, but only for small-amplitude waves, and thus, not accounting for wave-breaking processes. To address this gap, we perform experiments to probe inhomogeneous wave fields nearing the wave-breaking regime. We also show that by increasing the significant wave height towards the breaking limit, the kinetic energy grows faster than the variance of the surface elevation due to nonlinearity, providing a physical explanation why the occurrence of rogue wave first increases in shallower waters and suddenly decreases further shorewards.

I. INTRODUCTION

The forecast of extreme natural events is crucial for preventing loss of life, safeguarding infrastructure, and minimizing damage to both local and global environments. Over the past decades, climate extremes have also been intensely studied in addition to the most widely assessed natural hazards, such as earthquakes, tsunami or floods. Despite sailor stories, giant waves have been mostly overlooked throughout the nineteenth century [1]. However, since the New Year Wave of 1995 [2], rogue waves have been quickly recognized as a crucial natural hazard, responsible for considerable damage [3–5]. Wave loads due to rogue waves caused by abrupt inhomogeneities in the wave field have been recently examined and better assessed [6–8]. Models for short-term and long-term statistics of water waves are used to define the operating envelope for ocean vessels and fixed offshore structures. Moreover, the prediction and control of rogue waves are particularly important for marine and offshore safety. Among the various mechanisms of rogue wave formation and amplification, shoaling in coastal areas presents the highest hazardous risk [9].

Over the past decade, the out-of-equilibrium dynamics of rogue wave occurrence in random seas subject to shoaling have been intensively investigated [10–18]. Experiments have been carried out considering wave propagation either over a step or over relatively steep slopes,

and consistently showed the growth of steepness over the shoaling region, driving consequently anomalous wave statistics. Probability models have been obtained numerically [19] for surface elevation and theoretically [20] for wave crests, in both cases for a step, which constitutes the limiting condition of the shoal. Furthermore, a theoretical wave height distribution for steep shoals has been obtained [21], successfully describing experimental results [14, 22] for a variety of water depths and initial steepness values. However, these theories disregard wave breaking and are limited to relative water depths within second-order wave theories. To date, a proper analytical and continuous water wave solution for all water depths [23] is still missing, even for regular waves.

In an attempt to connect the two limiting conditions of a flat bottom and a step transition, an analysis of how the slope magnitude controls the extent of rogue wave amplification [24] and excess kurtosis of the wave height within the theory of small wave amplitude has emerged [25, 26]. Such theoretical reasoning agrees with the observation underlining that slopes not exceeding 1% cannot affect wave statistics [27]. The latter also shows that the amplification of rogue wave occurrence quickly saturates at slopes near 50% [13, 28]. All these results brought the second-order theoretical analysis of the effect of shoaling on rogue wave occurrence a step closer to a unified model for deep, intermediate and shallow water wave statistics. However, this treatment again calculated the magnitude of the slope effect in the absence of wave breaking. While there is no proper analytical and continuous water wave solution for all depths, we show that the ratio between significant wave height and water depth allows second-order wave theories to properly

* saulo.mendes@sjtu.edu.cn

† jerome.kasparian@unige.ch

‡ amin.chabchoub@oist.jp

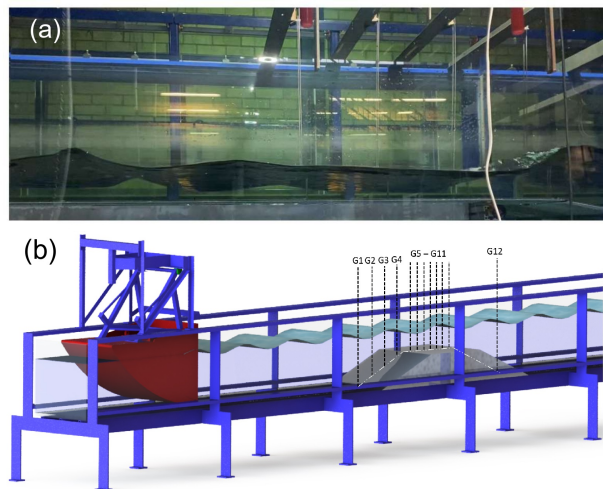


FIG. 1: (a) Photography of the experimental setup showing the wave gauge placements over the breakwater and (b) Experimental setup limited to the wave propagation region in the flume. The piston-type wave paddle on the left generates irregular waves according to Table I. A symmetric breakwater with a height of 0.4 m and length of 3 m is fixed near the paddle. The length of the breakwater's upper and horizontal plane is 1 m. The waves are fully dissipated by an artificial grass beach at the end of the flume. Please note that the surface elevation shown in the current sketch does not accurately represent the true physics of the generated wave. In a first configuration, we deploy eight gauges (G1-G7 and G12) in the first half of the breakwater and in a second configuration we move the gauges G4-G7 to the end of the plateau becoming then G8-G11.

describe rogue wave statistics in a regime otherwise belonging to cnoidal wave theory. We therefore verify the accuracy of this unified theory in flume experiments.

II. EXPERIMENTAL STUDY

A. Experimental design and setup

Laboratory experiments were carried out in a unidirectional wave flume installed at the University of Sydney (see figure 1a,b), in which irregular waves parameterizations with $\gamma = 3.3$ are generated by a wave paddle. The flume has dimensions of $30 \text{ m} \times 1 \text{ m} \times 1 \text{ m}$ and the water depth h can be varied from 0.2 to 0.8 m. A piston-type wavemaker can generate waves with frequencies ranging from 0.4 to 2 Hz. To mitigate reflection towards the region of the tank where the measurement is performed, an 8° -inclined beach covered with artificial grass is installed at the end of the flume. To analyze the statistical moments of out-of-equilibrium sea conditions induced by a submerged breakwater with identical up and down

slopes of $\nabla h = 1/5$, we record the temporal variation of surface elevation $\zeta(t)$ prior to, over, and after the breakwater. The experimental parameters, in particular the wave steepness and relative water depth, have been determined to cover regimes ranging from linear waves to breaking-dominated irregular seas [25]. A summary of all runs, described in Table I, can be assessed with regard to the physical regimes at play through the *Le Méhauté diagram*, see figure 2a [23], in which the water wave theories corresponding to different dimensionless water depth and significant wave height regimes are summarized, and the experimental runs are also specified. In this diagram, the initial and the predicted final state of the current experimental runs are shown by different line sections, evolving from right to left. It is shown that under most conditions, the significant wave height is expected to increase when the water depth decreases. $H_s/h \geq 0.8$ delineates the wave breaking regime [29, 30]. Visually, a small percentage of waves started to display plunging breakers atop the breakwater as early as for the conditions of run 5 ($\langle H_{s2}/h_2 \rangle \sim 0.5$), and spilling breakers were observed from run 4 onwards, with $\langle H_{s2}/h_2 \rangle \sim 0.4$. Conditions of run T were included to allow a direct comparison with previous experiments [14]. Each run was repeated for up to 12 realizations featuring 2500 waves each to ensure reproducibility and to compute the standard deviation of the excess kurtosis for each case. The adopted values follow the experimental requirements for convergence of the excess kurtosis [31].

Table I summarises the conditions for each run. The surface elevation as a function of time is calculated using a MATLAB code, and the corresponding control sequence of the wave paddle is generated through the Wave Synthesiser software [32, 33]. The sampling frequency of the data sent to the wave maker is set at 100 Hz, which is sufficient to accurately depict any wave envelope when considering the current wave paddle frequency limitation, as mentioned above, i.e. 0.4 to 2 Hz. In order to cover a wide range of propagation distances with a reasonable longitudinal resolution in spite of a limited number of available wave gauges, each run is successively performed following two gauge configurations: the first has seven wave gauges evenly spaced between the start of the up-slope until the mid-point of the breakwater plateau, whereas the second configuration has the last three gauges moved to the back end of this plateau (see the locations in figure 1b).

B. Results of water surface data acquisition

As shown in Table I, run 3 of the present experiments has similar values of both initial and final wave steepness $\epsilon = k_p H_s$ and relative water depth $k_p h$ as run T, and as such the spatial evolution of the excess kurtosis μ_4 of 3 is also similar to T. This strong amplification contrasts with the stability or drop in the exceedance probability observed on flat bottoms in similar conditions [34, 35].

Run	$k_{p1}h_1$	$k_{p2}h_2$	$k_{p1}H_{s1}$	H_{s1}	λ_{p1}	λ_{p2}	h_1	h_2	$\frac{H_{s1}}{h_1}$	$\langle \frac{H_{s2}}{h_2} \rangle$	$k_{p2}H_{s2}$	Waves
T	1.80	0.54	0.050	0.014	1.75	0.93	0.50	0.08	0.028	0.188	0.102	–
1	1.40	0.50	0.032	0.012	2.30	1.30	0.50	0.10	0.024	0.176	0.085	25,000
2	1.40	0.50	0.039	0.014	2.30	1.30	0.50	0.10	0.029	0.221	0.107	25,000
3	1.40	0.50	0.044	0.016	2.30	1.30	0.50	0.10	0.032	0.258	0.125	30,000
4	1.40	0.50	0.074	0.026	2.30	1.30	0.50	0.10	0.053	0.377	0.182	30,000
5	1.40	0.50	0.103	0.038	2.30	1.30	0.50	0.10	0.076	0.510	0.246	30,000
6	1.40	0.50	0.156	0.057	2.30	1.30	0.50	0.10	0.115	0.689	0.333	30,000
7	1.40	0.50	0.182	0.067	2.30	1.30	0.50	0.10	0.133	0.756	0.365	25,000
8	1.40	0.50	0.218	0.080	2.30	1.30	0.50	0.10	0.160	0.857	0.414	25,000
9	2.82	0.50	0.346	0.054	1.00	0.45	0.44	0.04	0.122	0.884	0.494	2,500
10	2.43	0.50	0.325	0.060	1.15	0.65	0.45	0.05	0.134	0.952	0.453	2,500

TABLE I: Summary of conditions before the shoal set for the wavemaker and atop the shoal for each run. Case T depicts the equivalent values of run 1 of Trulsen *et al.* [14] which were not experimentally tested. Each experimental realization was performed with 2500 waves, and for most runs we carried out 10-12 realizations with 2,500 waves each. Indices 1 and 2 stand for pre-shoal and top-of breakwater, respectively.

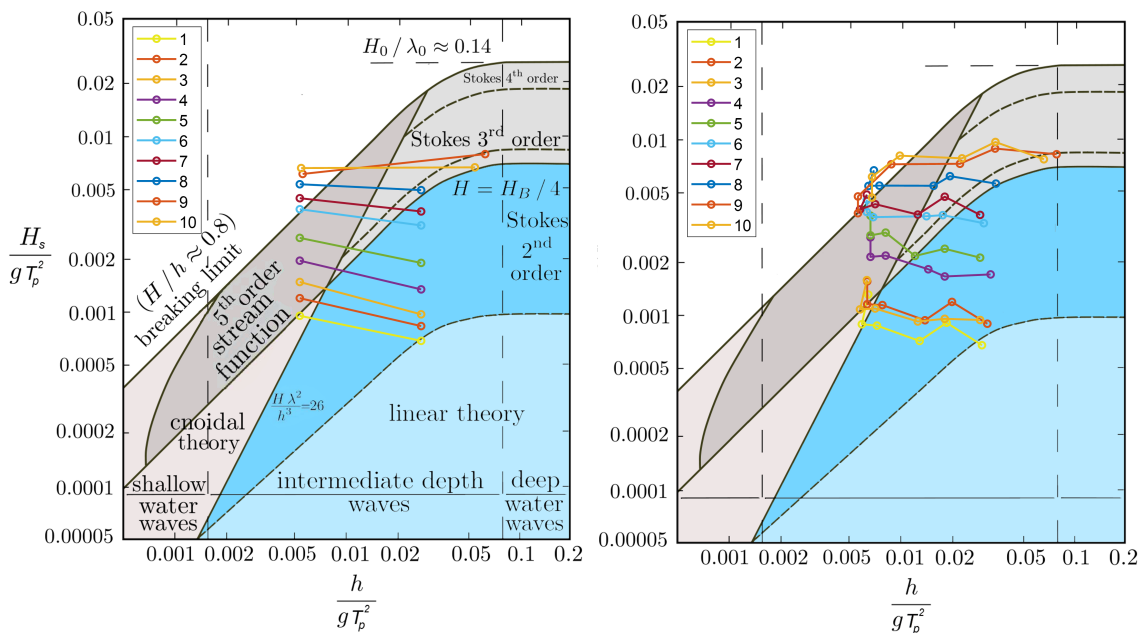


FIG. 2: Le Méhauté diagram with (Left) theoretical pre-shoal (rightmost point of the line) conditions and the wave train evolution over the breakwater (left point) for the 10 cases defined in Table I and (Right) with experimental results recorded in the aforementioned 10 cases. Each curve (from right to left) represents the spatial evolution of wave height with respect to the water depth over the breakwater. Note that for cases 1–8, the curves are generated based on measurements from gauges 1–5 and 7 with the maximum wave height occurring at gauges 7, while for cases 9 and 10, the curves are limited to gauges 1–6 due to early wave breaking. Background diagram adapted from Le Méhauté [23].

To verify the degree of wave breaking in each run described in Table I, we have plotted the evolution of the wave train overlaid on the Le Méhauté diagram (figure 2b) for all cases. We also plotted the spatial evolution of the energy spectrum for runs 1, 4, 6, and 9 in figure 3. The physical characteristics of all cases vary in such a way that we can consider them as consisting of four groups (1-3, 4-6, 7-8 and 9-10). Indeed the energy spectrum do not differ significantly between cases within

each group (similar steepness and relative water depth), therefore, we can summarize our findings in this regard in only four runs. When the initial wave steepness is relatively low, the JONSWAP spectral shape is preserved, with $\gamma = 3.3$ for all gauges along the up-slope and the first atop the shoal (runs 1-4). A much broader JONSWAP spectrum follows with increased presence of high frequencies. For larger initial wave steepness (run 6), the JONSWAP broadens already at the second wave gauge

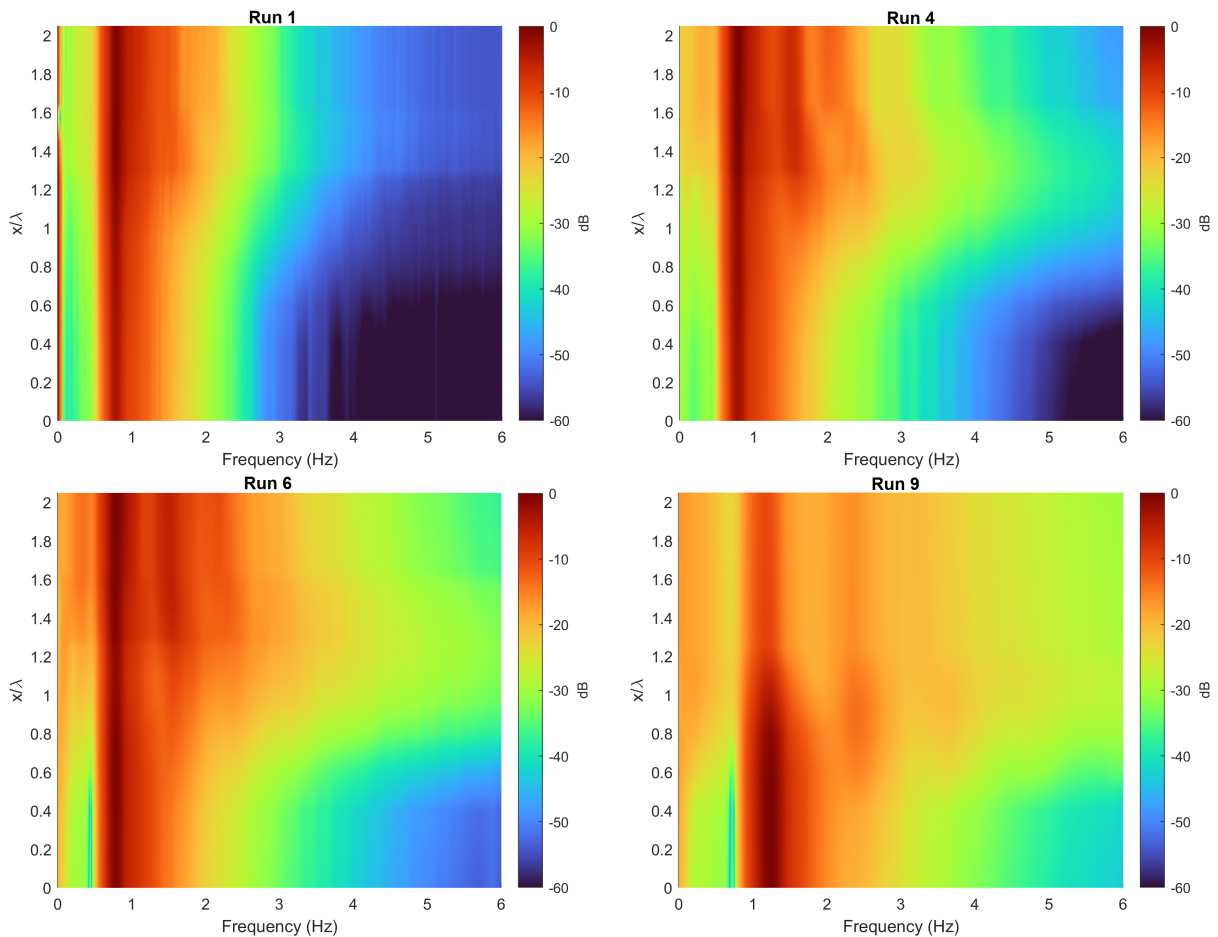


FIG. 3: Energy spectrum evolution over different gauges within the breakwater. See figure 1c and table I for the conditions of each run.

in the up-slope ($x = 0.6\lambda$). When most waves are breaking (runs 8-10) atop the breakwater ($x \gtrsim \lambda$), the spectrum is essentially flat except for a minor peak about $f_p \sim 1$ Hz, having shifted in about $\sim 20\%$ in comparison with runs of mild steepness such as run 2 and run 3. In addition, the spatio-temporal evolution of run 9 (figure 4 bottom right panel) displays the vertical asymmetry and sawtooth surface elevation characteristic of the surf zone [36], confirming the occurrence of wave breaking. This wave shape after gauge 4, i.e. $x/\lambda = 0.8$, is observed in all cases with steepness higher than or equal to run 5.

Note that we also observed a broadening of the wave spectrum over the shoal first due to the strong steepening of the waves. The delay in the narrowing of the spectrum can be explained by the decomposition of the wave field into cnoidal waves in the shallow area [37, 38].

C. Extreme Wave Statistics

Since the seminal *heuristic* work of Longuet-Higgins [39], the Rayleigh distribution is a model of the envelope of water waves and approximately also a good one for

wave heights. The rationale involved in this early work, which mostly borrows from the electromagnetic theory of signals [40], is most effective for a narrow-banded ocean spectrum [41]. Nonlinearities and a broader ocean spectrum effectively means that the central limit theorem has not been reached yet. In this case, asymptotic expansions for the normal law are needed [42]. However, they are treated as a refinement of the limited theory [39] but rather a further approximation when the assumptions thereof are not met [43]. Indeed, Longuet-Higgins [44] has shown that Edgeworth [45] series (also known as Gram-Charlier) can be applied, and the analytical expression for the surface elevation probability density can be described as a function of the excess in kurtosis. Partly due to the complexity of these types of distributions, the excess kurtosis is often used as a proxy to the evaluation of statistical distributions [46–48]. The latter is defined for a random variable X as,

$$\mu_4(X) = \frac{\mathbb{E}[X^4]}{(\mathbb{E}[X^2])^2} - 3 \quad , \quad (1)$$

where $\mathbb{E}[X]$ denotes the expectancy of X . In the context of shoaling small-amplitude waves, due to bound har-

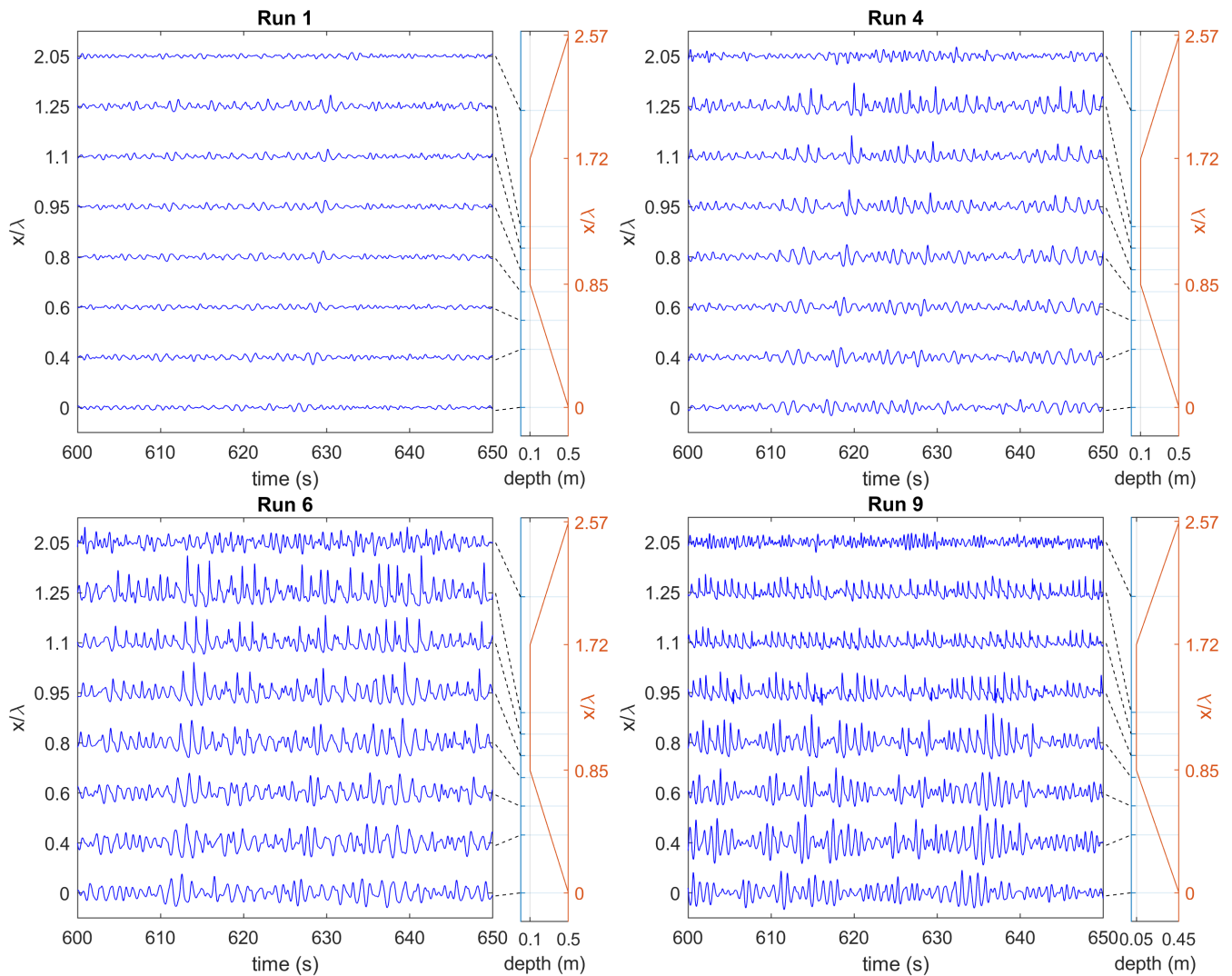


FIG. 4: Spatial evolution of the wave elevation time series over the breakwater for runs 1, 4, 6, and 9 of Table I, see title of each plot. The affiliating columns on the right of each plot indicate the gauge locations relative to the breakwater and the corresponding water depths (see figure 1b).

monics, the spatial evolution of kurtosis and the growth thereof is well understood and documented [16, 18, 20, 49]. The present study aims to assess how this phenomenon responds to wave steepness up to the regime where wave breaking becomes dominant. In other words, we want to investigate whether it is possible to describe the peak in excess kurtosis atop a shoal regardless of the class of wave theories (linear, second-order, third-order, cnoidal etc.), which is one of the last gaps left in this problem from an analytical point of view.

In figure 5 we observe the maximum excess kurtosis atop the breakwater as a function of the wave steepness observed at the same position, taking into account the spectral shift, for the two wave gauge configurations. We find a steep rise of the peak in excess kurtosis for increasing wave steepness up to the point in which wave breaking starts ($k_{p2}H_{s2} \sim 0.25$), followed by a decay by 25–45%.

Our results contrast with the aforementioned flat-bottom and mild slope results [34, 35], which observe a five to six times smaller peak in excess kurtosis, as well as a much stronger decay in excess kurtosis ($> 100\%$) towards negative values when wave breaking is dominant. The likely source for this different behavior is the milder slope in Xu *et al.* [34] and Karpadakis *et al.* [35] than in our experiments. Moreover, it is possible that the water depth was not sufficiently shallow to drop the excess kurtosis below zero.

Indeed, at least for unidirectional deep or intermediate water conditions, the breaking threshold of steep Stokes waves dominated by modulational instability may be larger than predicted by empirical models, see for instance Section 5.2 of Babanin [50]. This breaking threshold may increase even further when considering shallower depths [51] and wave directionality in finite wa-

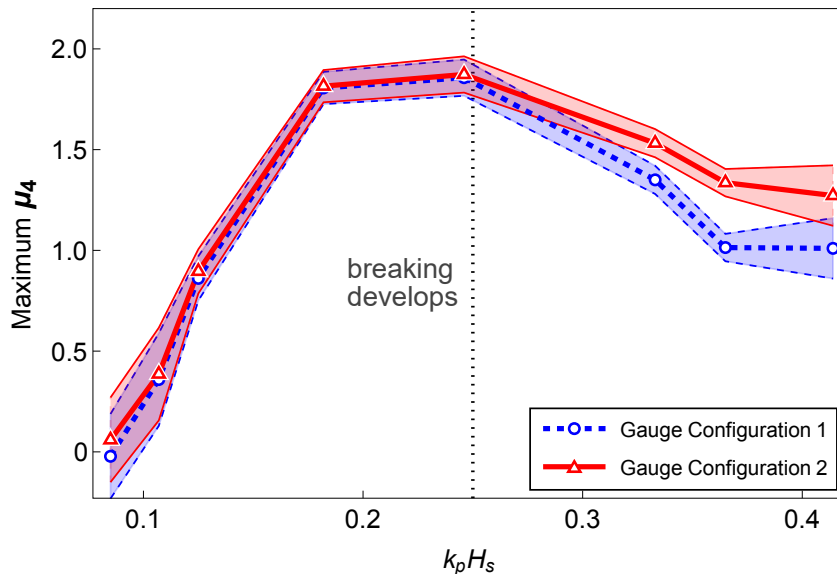


FIG. 5: Maximum observed excess kurtosis atop the shoal for each run (mean of realizations) as a function of the local wave steepness $k_p H_s$ at that location. The shaded areas correspond to the 95% confidence intervals. The vertical dotted line highlights the run with the lowest wave steepness, in which wave breaking appears.

ter regimes [52]. We also would like to highlight that a quantitative approach to determine wave breaking dissipation is achieved when conducting large eddy [53] or direct numerical simulations [54]. However, in view of the number of waves and duration of the processes, this is very challenging to undertake.

III. UNIFIED THEORETICAL ANALYSIS FOR WAVE STATISTICS

In this section we briefly review, for the sake of being self-contained, the stationary and non-homogeneous treatment of ocean statistics in section III A. Then, in section III B we propose a unifying method that approximates the statistical behavior of finite-amplitude waves even up to wave breaking building on the framework of section III A.

A. Stationary, Non-homogeneous Treatment of Ocean Statistics

Following Mendes *et al.* [49] we start by considering the total energy per width contained within a wavelength:

$$\rho g \mathcal{E} = \frac{\rho}{2\lambda} \int_0^\lambda \left[g(\zeta + h)^2 + \int_{-h(x)}^\zeta (u^2 + w^2) dz \right] dx \quad (2)$$

where ρ is the density, g is the gravitational acceleration, λ the zero-crossing wavelength, h the water column depth, x the direction of motion and z the vertical axis, ζ is the sea surface elevation and $u = \partial\Phi/\partial x$ and

$w = \partial\Phi/\partial z$ are the velocity components derived from the velocity potential Φ .

We assume that the statistical properties and homogeneity of a wave train traveling over a flat bottom are well described by the linear wave theory. We assume stationarity in time but consider spatial non-homogeneity. The Gaussian statistics of the initial wave train will be affected as soon as the wave train feels the bathymetry. Consequently, its exceeding probability \mathcal{R}_α will be transformed into $\mathcal{R}_{\alpha,\Gamma}$ during a sufficiently unsteady shoaling process with an asymmetry \mathfrak{S} between crests and troughs:

$$\mathcal{R}_\Gamma(H > \alpha H_s) = e^{-2\alpha^2/\mathfrak{S}^2\Gamma} \quad , \quad \Gamma = \frac{\langle \zeta^2 \rangle}{\mathfrak{e}} \quad , \quad (3)$$

with $\langle \zeta^2 \rangle$ denoting the variance of the surface elevation, H the wave height, and H_s the significant wave height, defined as average among the third-highest waves.

B. Approximate Analytical Solution for Finite Amplitude Waves

For finite amplitude waves, unlike previously in the previous subsection, we must compute a finite upper bound of the vertical integration in the kinetic energy formulation of eq (2). The upper bound of eq (2) is introduced in textbooks for harmonic waves and carried out to general irregular waves without a proper discussion of its validity. The usual upper bound of integration taken to be the $\zeta(x, t)$ is not strictly correct in the case of shoaling: over the region of the spatial averaging of the kinetic energy the surface elevation will not be a representative measure of the sea state unless we extend the

interval of integration in x to a very large spatial series, which may extend far beyond the shoaling length itself. Much like one has to use a representative measure for the wavelength, in this case the zero-crossing measure, one must then find a representative average measure for the surface elevation as an upper bound. Naturally, since Gaussian seas are zero-mean and oscillations around this value are tiny due to low nonlinearity, the rms mean is the proper choice. In a typical Gaussian sea, which implies a Rayleigh distribution of wave heights, the most likely waves have height $H = 0.5H_s$ while the mean height approximately amounts to $0.6H_s$.

A significant increase in the ratio H_s/h affects the kinetic term within the total energy. Hence, we have to fully evaluate the second integral in eq. (2). If we consider this increase in significant wave height, we can no longer use the assumption and delimitation $\zeta \ll H_s$ in our previous work [25, 26]. However, a rather strict application of the Γ correction to the wave theory delimitation diagram introduced by Le Méhauté [23], See Figure 2 would suggest the co-existence of several piecewise formulations for Γ delimited together by criteria related to the Ursell number, mean steepness and wave breaking. Unfortunately, a continuous formulation connecting all versions of Γ for each wave theory of Le Méhauté's diagram is simply unfathomable, since the task of unifying all water wave solutions is yet to be accomplished [55, 56]. Practical applications of the cnoidal wave theory and the Γ parameter thereof are also very difficult to deal with from an engineering perspective because it contains the Jacobian elliptic functions and the complete elliptic integrals of the first and second kinds [57–59]. Therefore, it would not serve us at all to compute piecewise formulations of Γ , particularly if our goal is to provide a unified picture of rogue wave occurrence from deep or finite depth waters to shallow waters from low to very high steepness, and from low to high height-to-depth ratios. Inevitably, we shall hold to the unification of the stochastic behavior of irregular waves grounded on foundational integral properties of water waves, namely their normalized variance and total spectral energy.

That said, because the maximum and minimum of the surface elevation are of the same order of magnitude in this case, we expect the most likely range of oscillation $-1/4 < \zeta/H_s < 1/4$ which is also representative of the spatial series. Naturally, even in weakly nonlinear seas the oscillations will not be symmetrical between

the wave crest and trough, as the ratio between them grows monotonically with normalized height, see figure 31 of Mendes *et al.* [21]. Even for rogue waves the ratio between nonlinear crest to its height is on average 20% higher than in a symmetrical sea, so that the wave asymmetry would hardly impact the upper bound for the integration of the kinetic energy. In contrast, ordinarily tall crests don't exceed the symmetrical sea case in more than 10% [21, 26]. This range is of course compatible with the root-mean-square surface elevation of $\sqrt{\langle \zeta^2 \rangle} = \sigma = H_s/4$. Therefore, we start the evaluation of the kinetic spectral energy by integrating up to an upper bound representative of the bulk of waves:

$$\mathcal{E}_k \approx \frac{1}{2\lambda g} \int_0^\lambda \int_{-h(x)}^{H_s/4} \left[\left(\frac{\partial \Phi}{\partial x} \right)^2 + \left(\frac{\partial \Phi}{\partial z} \right)^2 \right] dz dx \quad , \quad (4)$$

Defining the variables $\varphi = k(z+h)$, $\Lambda = kh$ and $\phi = kx - \omega t$, the second-order regular wave velocity potential can be written as:

$$\Phi(x, z, t) = \frac{a\omega \cosh \varphi}{k \sinh \Lambda} \sin \phi + \left(\frac{3ka}{8} \right) \frac{a\omega \cosh(2\varphi)}{k \sinh^4 \Lambda} \sin(2\phi) \quad . \quad (5)$$

Ergo, the surface elevation becomes:

$$\zeta(x, t) = a \cos \phi + \frac{ka}{4} \sqrt{\tilde{\chi}_1} a \cos(2\phi) \quad , \quad (6)$$

where $\tilde{\chi}_1 = (3 - \tanh^2 \Lambda)^2 / \tanh^6 \Lambda$ is the super-harmonic term. If we ignore the gradient of variables such as wavelength, the following expressions hold for the vertical velocity:

$$\begin{aligned} u_0 &= a\omega \left\{ \frac{\cosh \varphi}{\sinh \Lambda} \cos \phi + \left(\frac{3ka}{4} \right) \frac{\cosh(2\varphi)}{\sinh^4 \Lambda} \cos(2\phi) \right\} \quad , \\ w &= a\omega \left\{ \frac{\sinh \varphi}{\sinh \Lambda} \sin \phi + \left(\frac{3ka}{4} \right) \frac{\sinh(2\varphi)}{\sinh^4 \Lambda} \sin(2\phi) \right\} \quad (7) \end{aligned}$$

We know that the kinetic energy of the gradient-free term leads to [49]:

$$\mathcal{E}_{k0} \approx \frac{1}{2\lambda g} \int_0^\lambda \int_{-h}^{H_s/4} (u_0^2 + w^2) dx dz \quad , \quad (8)$$

Since the integrals of cross-order terms $\sin \phi \sin(2\phi)$ and $\cos \phi \cos(2\phi)$ of eq. (8) vanish, we have:

$$\begin{aligned} \mathcal{E}_{k0} &= \frac{(a\omega)^2}{2\lambda g} \int_0^\lambda \int_{-h}^{H_s/4} \left[\frac{\cosh^2 \varphi}{\sinh^2 \Lambda} \cos^2 \phi + \left(\frac{3ka}{4} \right)^2 \frac{\cosh^2(2\varphi)}{\sinh^8 \Lambda} \cos^2(2\phi) \right. \\ &\quad \left. + \frac{\sinh^2 \varphi}{\sinh^2 \Lambda} \sin^2 \phi + \left(\frac{3ka}{4} \right)^2 \frac{\sinh^2(2\varphi)}{\sinh^8 \Lambda} \sin^2(2\phi) \right] dx dz \quad , \\ &= \frac{a^2 \cdot gk \tanh \Lambda}{4g \sinh^2 \Lambda} \int_{-h}^{H_s/4} \left[\cosh^2 \varphi + \sinh^2 \varphi + \left(\frac{3ka}{4} \right)^2 \frac{\cosh^2(2\varphi) + \sinh^2(2\varphi)}{\sinh^6 \Lambda} \right] dz \quad , \end{aligned} \quad (9)$$

Noting that a transformation of steepness between regular and irregular wave fields obey $ka \rightarrow \pi\varepsilon\mathfrak{S} \approx \sqrt{2}k_p H_s \mathfrak{S}$

[49], the above integral is approximated for the regime of interest ($\Lambda \leq 2$, $k_p H_s \leq 1/4$):

$$\begin{aligned} \mathcal{E}_{k0} &\approx \frac{a^2}{4} \frac{2k}{\sinh(2\Lambda)} \left[\frac{\sinh(2\Lambda) + \sinh(\frac{1}{2}k_p H_s)}{2k} + \left(\frac{3\pi\varepsilon\mathfrak{S}}{4} \right)^2 \frac{\sinh(4\Lambda) + \sinh(k_p H_s)}{4k \sinh^6 \Lambda} \right], \\ &\approx \frac{a^2}{4} \left[1 + \frac{\sinh(\frac{1}{2}k_p H_s)}{\sinh(2\Lambda)} + \left(\frac{\pi\varepsilon\mathfrak{S}}{4} \right)^2 \chi_1 \left(1 + \frac{\sinh(k_p H_s)}{\sinh(4\Lambda)} \right) \right], \end{aligned} \quad (10)$$

where we have denoted $\chi_1 = 9 \cosh(2\Lambda) \sinh^{-6} \Lambda$. Due to the fact that $k_p H_s/2 \leq 1/4$ (wave breaking threshold), we can approximate $\sinh(\frac{1}{2}k_p H_s)$ as $\frac{1}{2} \sinh(k_p H_s)$ with an error of less than 2% to simplify the calculations. The finite-amplitude gradient-free kinetic energy is best approximated in intermediate water,

$$\mathcal{E}_{k0} \approx \frac{a^2}{4} \left[1 + \left(\frac{\pi\varepsilon\mathfrak{S}}{4} \right)^2 \chi_1 \right] \left[1 + \frac{\sinh(k_p H_s)}{\sinh(4\Lambda)} \right]. \quad (11)$$

The corrections of the type $\sinh(k_p H_s)/\sinh(4\Lambda)$ due to finite-amplitude waves is the only difference to the main result of Mendes *et al.* [49]. In the narrow range in relative water depth ($\Lambda \sim 0.2$) where extreme wave statistics

are strongly amplified due to shoaling [18], the finite-amplitude correction within the last pair of brackets on the r.h.s of eq. (11) reduces to $1 + H_s/(4h)$. As such, the finite-amplitude correction will only become relevant if $H_s \gtrsim 0.4h$. This ratio was considerably smaller in the experiments reported in Trulsen *et al.* [14], and did not exceed this threshold in other similar studies [12, 20]. However, in deep water the term $\sinh(4\Lambda)$ grows rapidly, and regardless of how large H_s/h is, the finite-amplitude correction to the kinetic energy is negligible.

On the other hand, partial derivatives of the variables (h, k, λ) will arise in the direction of motion in addition to the textbook solution for u_0 [60, 61]. Noting that $\nabla\phi = k + x\nabla k$ and $\nabla\varphi = (z+h)\nabla k + k\nabla h$, the horizontal velocity becomes:

$$\begin{aligned} \frac{ku}{a\omega} &= \left(-\frac{\nabla k}{k} \right) \frac{\cosh \varphi}{\sinh \Lambda} \sin \phi + \nabla\varphi \cdot \frac{\sinh \varphi}{\sinh \Lambda} \sin \phi - \nabla\Lambda \frac{\cosh \Lambda}{\sinh \Lambda} \cdot \frac{\cosh \varphi}{\sinh \Lambda} \sin \phi + \nabla\phi \cdot \frac{\cosh \varphi}{\sinh \Lambda} \cos \phi \\ &+ \left(\frac{3ka}{8} \right) \left[\left(-\frac{\nabla k}{k} \right) \frac{\cosh(2\varphi)}{\sinh^4 \Lambda} \sin(2\phi) + 2\nabla\varphi \cdot \frac{\sinh(2\varphi)}{\sinh^4 \Lambda} \sin(2\phi) \right. \\ &\left. - 4\nabla\Lambda \frac{\cosh \Lambda}{\sinh \Lambda} \cdot \frac{\cosh(2\varphi)}{\sinh^4 \Lambda} \sin(2\phi) + 2\nabla\phi \cdot \frac{\cosh(2\varphi)}{\sinh^4 \Lambda} \cos(2\phi) \right], \end{aligned} \quad (12)$$

being expanded and compared to the otherwise gradient-

free velocity u_0 :

$$\begin{aligned} \frac{u}{a\omega} &= \left\{ \frac{\cosh \varphi}{\sinh \Lambda} \cos \phi + \left(\frac{3ka}{4} \right) \frac{\cosh(2\varphi)}{\sinh^4 \Lambda} \cos(2\phi) \right\} + \frac{x\nabla k}{k} \frac{\cosh \varphi}{\sinh \Lambda} \cos \phi - \frac{\nabla k}{k^2} \frac{\cosh \varphi}{\sinh \Lambda} \sin \phi \\ &+ \left((z+h) \frac{\nabla k}{k} + \nabla h \right) \frac{\sinh \varphi}{\sinh \Lambda} \sin \phi - \left(h \frac{\nabla k}{k} + \nabla h \right) \frac{\cosh \Lambda}{\sinh \Lambda} \cdot \frac{\cosh \varphi}{\sinh \Lambda} \sin \phi \\ &+ \left(\frac{3ka}{4} \right) \left[\frac{x\nabla k}{k} \frac{\cosh(2\varphi)}{\sinh^4 \Lambda} \cos(2\phi) - \frac{1}{2} \frac{\nabla k}{k^2} \frac{\cosh(2\varphi)}{\sinh^4 \Lambda} \sin(2\phi) \right. \\ &\left. + \left((z+h) \frac{\nabla k}{k} + \nabla h \right) \frac{\sinh(2\varphi)}{\sinh^4 \Lambda} \sin(2\phi) - \left(h \frac{\nabla k}{k} + \nabla h \right) \frac{2 \cosh \Lambda}{\sinh \Lambda} \cdot \frac{\cosh(2\varphi)}{\sinh^4 \Lambda} \sin(2\phi) \right] \\ &\equiv \frac{u_0 + \Delta u}{a\omega}. \end{aligned} \quad (13)$$

Small finite-amplitude corrections to the kinetic energy

due to the gradient of the physical variables across the

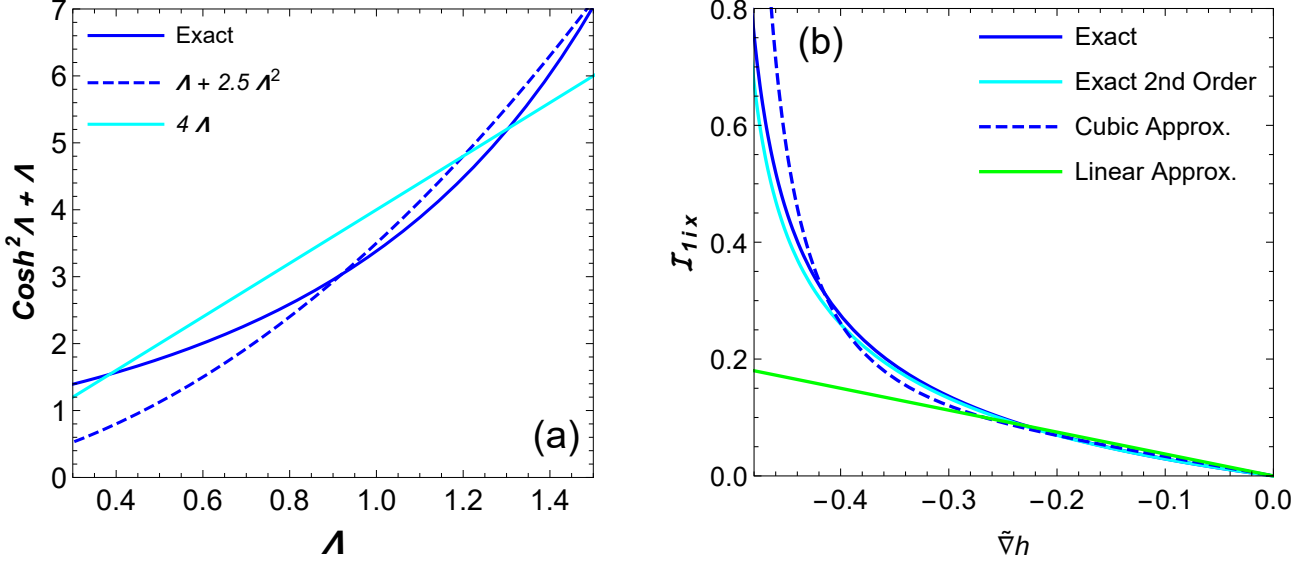


FIG. 6: (a) Polynomial approximations for the denominator of eq. (18) and (b) Resulting numerical value of different levels of approximations for the integral in eq. (23).

shoal become,

$$\Delta \mathcal{E}_k \equiv \mathcal{E}_k - \mathcal{E}_{k0} \approx \frac{1}{2\lambda g} \int_0^\lambda \int_{-h}^{H_s/4} (2u_0 \Delta u + (\Delta u)^2) dx dz \quad . \quad (14)$$

Recalling eq. (13) and that cross-order trigonometric

functions vanish after integration, as well as $\nabla k/k = -\nabla \lambda/\lambda$, we find:

$$\begin{aligned} \Delta \mathcal{E}_k &= \frac{(a\omega)^2}{2\lambda g} \int_0^\lambda \int_{-h}^{H_s/4} dx dz \left\{ -2x \frac{\nabla \lambda}{\lambda} \left[\frac{\cosh^2 \varphi}{\sinh^2 \Lambda} \cos^2 \phi + \left(\frac{3ka}{4} \right)^2 \frac{\cosh^2(2\varphi)}{\sinh^8 \Lambda} \cos^2(2\phi) \right] \right. \\ &+ \left[\frac{\cosh^2 \varphi}{\sinh^2 \Lambda} \cos^2 \phi + \left(\frac{3ka}{4} \right)^2 \frac{\cosh^2(2\varphi)}{\sinh^8 \Lambda} \cos^2(2\phi) \right] \left(x \frac{\nabla \lambda}{\lambda} \right)^2 + \left[\frac{\cosh^2 \varphi}{\sinh^2 \Lambda} \sin^2 \phi + \left(\frac{3ka}{4} \right)^2 \frac{\cosh^2(2\varphi)}{4 \sinh^8 \Lambda} \sin^2(2\phi) \right] \left(\frac{\nabla \lambda}{2\pi} \right)^2 \\ &+ \left[\frac{\sinh^2 \varphi}{\sinh^2 \Lambda} \sin^2 \phi + \left(\frac{3ka}{4} \right)^2 \frac{\sinh^2(2\varphi)}{\sinh^8 \Lambda} \sin^2(2\phi) \right] \left(\nabla h - (z+h) \frac{\nabla \lambda}{\lambda} \right)^2 \\ &+ \left[\frac{\cosh^2 \varphi}{\sinh^2 \Lambda} \sin^2 \phi + \left(\frac{3ka}{4} \right)^2 \frac{4 \cosh^2(2\varphi)}{\sinh^8 \Lambda} \sin^2(2\phi) \right] \left(h \frac{\nabla \lambda}{\lambda} - \nabla h \right)^2 \frac{\cosh^2 \Lambda}{\sinh^2 \Lambda} \\ &+ \left[\frac{\sinh(2\varphi)}{\sinh^2 \Lambda} \sin^2 \phi + \left(\frac{3ka}{4} \right)^2 \frac{\sinh(4\varphi)}{2 \sinh^8 \Lambda} \sin^2(2\phi) \right] \frac{\nabla \lambda}{2\pi} \left(\nabla h - (z+h) \frac{\nabla \lambda}{\lambda} \right) \\ &+ \left[\frac{\cosh^2 \varphi}{\sinh^2 \Lambda} \sin^2 \phi + \left(\frac{3ka}{4} \right)^2 \frac{\cosh^2(2\varphi)}{\sinh^8 \Lambda} \sin^2(2\phi) \right] \frac{\nabla \lambda}{2\pi} \left(h \frac{\nabla \lambda}{\lambda} - \nabla h \right) \frac{\cosh \Lambda}{\sinh \Lambda} \\ &+ \left[\frac{\sinh(2\varphi)}{\sinh^2 \Lambda} \sin^2 \phi + \left(\frac{3ka}{4} \right)^2 \frac{2 \sinh(4\varphi)}{\sinh^8 \Lambda} \sin^2(2\phi) \right] \frac{\cosh \Lambda}{\sinh \Lambda} \times \left(\nabla h - (z+h) \frac{\nabla \lambda}{\lambda} \right) \left(h \frac{\nabla \lambda}{\lambda} - \nabla h \right) \\ &\equiv \frac{(a\omega)^2}{2g \sinh^2 \Lambda} \sum_{i=1}^8 \mathcal{I}_i \approx \frac{ka^2}{\sinh(2\Lambda)} \sum_{i=1}^8 \mathcal{I}_i \quad . \end{aligned} \quad (15)$$

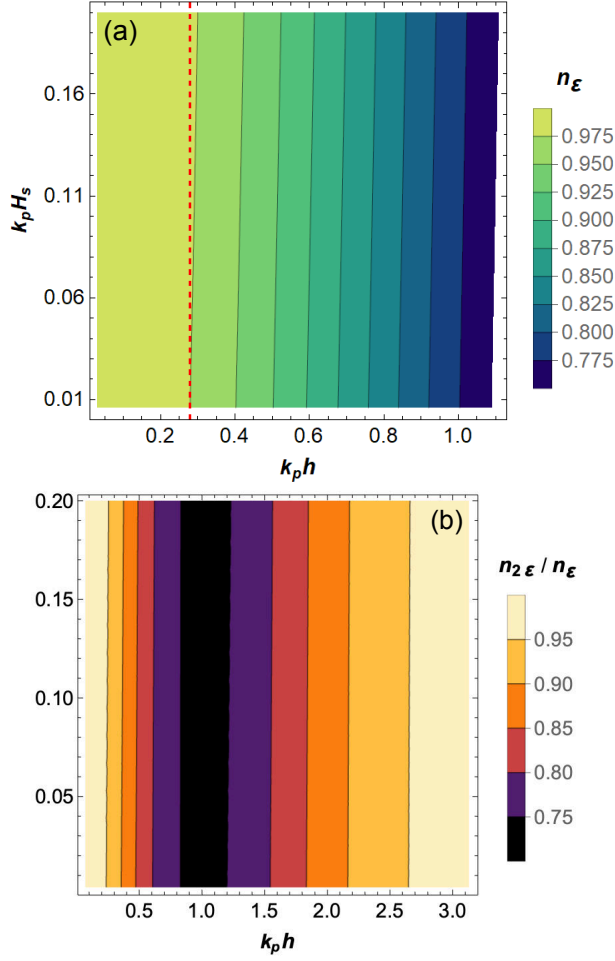


FIG. 7: Behavior of the steepness-dependent ratio between group and phase velocities ($n_\epsilon, n_{2\epsilon}$). The red dashed vertical line depicts the contour line of n as if it were not steepness-dependent.

From the dispersion relation, we know that for a pre-shoal wave period T_0 the shoaling causes a spatial variation in the wavelength, namely:

$$\lambda(x) = \frac{gT_0^2}{2\pi} \tanh(k(x)h(x)) \quad . \quad (16)$$

Then, the derivative along the direction of motion is applied to the wavelength, reading:

$$\nabla\lambda = \lambda_0 \nabla \left[\tanh(k(x)h(x)) \right] = \frac{\lambda_0}{\cosh^2 \Lambda(x)} \left[k(x) \nabla h + h(x) \nabla k \right] \quad . \quad (17)$$

Because of the identity $\nabla k/k = -(\nabla\lambda/\lambda)$, the wavelength gradient reads:

$$\begin{aligned} \nabla\lambda &= \frac{2\pi \nabla h}{\cosh^2 \Lambda(x) + \Lambda(x)}, \\ &= \frac{2\pi \nabla h}{\cosh^2 \left[kh_0 \left(1 + \frac{x \nabla h}{h_0} \right) \right] + kh_0 \left(1 + \frac{x \nabla h}{h_0} \right)} \quad . \quad (18) \end{aligned}$$

We linearize the by linearly fitting $\cosh^2 \Lambda + \Lambda \approx 4\Lambda$ (figure 6a), such that:

$$\begin{aligned} \nabla\lambda &\approx \frac{\pi}{2} \frac{\nabla h}{kh} \approx \frac{\pi}{2} \cdot \frac{\nabla h}{kh_0 \left(1 + \frac{x \nabla h}{h_0} \right)} \\ &\equiv \frac{\tilde{\nabla} h}{2 \left(1 + \frac{2x}{\lambda} \tilde{\nabla} h \right)} \equiv \frac{\tilde{\nabla} h}{2f(x, \tilde{\nabla} h)}, \quad (19) \end{aligned}$$

where,

$$\tilde{\nabla} h = \frac{\pi \nabla h}{kh_0} \quad . \quad (20)$$

Evidently, all integrals will result in functions of the order of ∇h or $(\nabla h)^2$ because the gradient $\nabla\lambda$ somewhat depends on the former. Thus, even before integration, we expect that corrections to eq. (11) due to the spatial gradients of the wavelength and water depth will be quite small, with the leading term coming from \mathcal{I}_1 . According to the approximated wavelength gradient above, we perform the step-by-step computation of \mathcal{I}_1 whilst implementing the transformation from regular to irregular waves upfront without any loss of generality:

$$\begin{aligned} \mathcal{I}_1 &\approx -\frac{2}{\lambda^2} \int_0^\lambda \int_{-h}^{H_s/4} dx dz x \nabla\lambda \left[\cosh^2 \varphi \cos^2 \phi + \left(\frac{\pi \epsilon \mathfrak{G}}{4} \right)^2 \chi_1 \frac{\cosh^2(2\varphi)}{\cosh(2\Lambda)} \cos^2(2\phi) \right] \quad , \quad (21) \\ &\approx -\frac{\tilde{\nabla} h}{\lambda^2} \int_0^\lambda \int_{-h}^{H_s/4} \left[\cosh^2 \varphi \cos^2 \phi + \left(\frac{\pi \epsilon \mathfrak{G}}{4} \right)^2 \chi_1 \frac{\cosh^2(2\varphi)}{\cosh(2\Lambda)} \cos^2(2\phi) \right] \frac{x dx dz}{\left(1 + \frac{2x}{\lambda} \tilde{\nabla} h \right)}. \end{aligned}$$

The lowest order in steepness has a spatial function:

$$\mathcal{I}_{11x} = -\frac{\tilde{\nabla} h}{\lambda^2} \int_0^\lambda \frac{x \cos^2 \phi}{\left(1 + \frac{2x}{\lambda} \tilde{\nabla} h \right)} dx \quad , \quad (22)$$

that can be approximated as a polynomial (figure 6b):

$$\mathcal{I}_{11x} \approx -\frac{\tilde{\nabla} h}{3} \left[1 - \frac{3(\tilde{\nabla} h)^3}{(1 + 2\tilde{\nabla} h)} \right] \cong -\frac{3\tilde{\nabla} h}{8} \equiv f_1(\tilde{\nabla} h). \quad (23)$$

The second-order term reads:

$$\mathcal{I}_{12x} = -\frac{\tilde{\nabla}h}{\lambda^2} \int_0^\lambda \frac{x \cos^2(2\phi)}{\left(1 + \frac{2x}{\lambda} \tilde{\nabla}h\right)} dx \quad . \quad (24)$$

Since $\cos^2 \phi$ and $\cos^2 2\phi$ oscillate much faster than the evolution of x , we expect that $\mathcal{I}_{12x} \approx \mathcal{I}_{11x}$. Note that the term $1 + 2\tilde{\nabla}h$ appears in the non-trivial integration, thus also in the approximation. It can be verified that $0.95 \leq \mathcal{I}_{12x}/\mathcal{I}_{11x} \leq 1$ in the interval $\tilde{\nabla}h > -0.4$, the latter being the upper limit for the theory of arbitrary slopes [25]. As such, the leading term in the gradient-dependent correction to the kinetic energy becomes,

$$\Delta \mathcal{E}_k \sim f_1(\tilde{\nabla}h) \frac{(a\omega)^2}{2g \sinh^2 \Lambda} \times \int_{-h}^{\frac{H_s}{4}} \left[\cosh^2 \varphi + \left(\frac{\pi \varepsilon \mathfrak{G}}{4}\right)^2 \frac{\chi_1 \cosh^2(2\varphi)}{\cosh(2\Lambda)} \right] dz \quad , \quad (25)$$

whose application of the algebraic manipulation in eqs. (10-10) leads to:

$$\Delta \mathcal{E}_k \sim f_1(\tilde{\nabla}h) \frac{a^2}{4} \left[\left(1 + \frac{\sinh(\frac{1}{2}k_p H_s)}{\sinh(2\Lambda)}\right) n_\varepsilon + \left(\frac{\pi \varepsilon \mathfrak{G}}{4}\right)^2 \chi_1 \left(1 + \frac{\sinh(k_p H_s)}{\sinh(4\Lambda)}\right) n_{2\varepsilon} \right] \quad , \quad (26)$$

where the group-to-phase velocity ratios read,

$$n_\varepsilon = \frac{1}{2} \left[1 + \frac{2\Lambda + \frac{1}{2}k_p H_s}{\sinh(2\Lambda) + \sinh(\frac{1}{2}k_p H_s)} \right] ; \quad n_{2\varepsilon} = \frac{1}{2} \left[1 + \frac{4\Lambda + k_p H_s}{\sinh(4\Lambda) + \sinh(k_p H_s)} \right] \quad . \quad (27)$$

Naturally, in the limit of deep water linear (Airy) waves ($\Lambda \rightarrow \infty, \varepsilon \rightarrow 0$) we find that $n_\varepsilon = n = n_{2\varepsilon} = n_2 = 1/2$, where n is defined as the ratio between group and phase velocities [29], and the kinetic energy reads:

$$\Delta \mathcal{E}_k \approx \frac{a^2}{4} \left[n_\varepsilon + n_{2\varepsilon} \left(\frac{\pi \varepsilon \mathfrak{G}}{4}\right)^2 \chi_1 \right] \times \left[1 + \frac{\sinh(k_p H_s)}{\sinh(4\Lambda)} \right] f_1(\tilde{\nabla}h) \quad . \quad (28)$$

As shown in figure 7, the effect of steepness is tiny on the group velocity ratios. Therefore, n (resp. n_ε) deviate at most by 1% (resp. 4%) from n_2 (resp $n_{2\varepsilon}$) for $k_p H_s = 0.2$ in intermediate water and vanishing otherwise. As such, we may greatly simplify the kinetic energy correction:

$$\Delta \mathcal{E}_k \sim \frac{a^2}{4} \left[1 + \left(\frac{\pi \varepsilon \mathfrak{G}}{4}\right)^2 \chi_1 \right] \times \left[1 + \frac{\sinh(k_p H_s)}{\sinh(4\Lambda)} \right] f_1(\tilde{\nabla}h) n \quad . \quad (29)$$

Moreover, the remaining integrals $I_i (i > 1)$ of eq. (15) will, to leading order, affect only the function $f_1(\tilde{\nabla}h)$. In fact, the velocity ratio n_ε will appear in all linear terms $I_{i1x} (i > 1)$ and likewise $n_{2\varepsilon}$ to all nonlinear terms $I_{i2x} (i > 1)$. Consequently, the computation of all remaining integrals borders a futile exercise, as all other integrals are negligible. Hence, taking into account corrections due to the finite amplitude of waves and the gradient of wave variables along the shoal, we recalculate the total energy density consisting of potential and kinetic counterparts:

$$\mathcal{E} = \mathcal{E}_p + \mathcal{E}_{k0} + \Delta \mathcal{E}_k \quad . \quad (30)$$

Borrowing from Section 3.1 of Mendes *et al.* [49], the total energy density now reads:

$$\begin{aligned} \frac{4\mathcal{E}}{a^2} &\approx 1 + \left(\frac{\pi \varepsilon \mathfrak{G}}{4}\right)^2 \tilde{\chi}_1 + \left[1 + \left(\frac{\pi \varepsilon \mathfrak{G}}{4}\right)^2 \chi_1 \right] \left[1 + \frac{\sinh(k_p H_s)}{\sinh(4\Lambda)} \right] \left[1 + f_1(\tilde{\nabla}h) n \right] \quad , \quad (31) \\ &\approx 2 + f_1(\tilde{\nabla}h) n + \frac{\sinh(k_p H_s)}{\sinh(4\Lambda)} \left[1 + f_1(\tilde{\nabla}h) n \right] + \left(\frac{\pi \varepsilon \mathfrak{G}}{4}\right)^2 \left\{ \tilde{\chi}_1 + \chi_1 \left[1 + \frac{\sinh(k_p H_s)}{\sinh(4\Lambda)} \right] \left[1 + f_1(\tilde{\nabla}h) n \right] \right\} \quad , \end{aligned}$$

such that to leading order,

$$\frac{2\mathcal{E}}{a^2} \approx 1 + \frac{f_1(\tilde{\nabla}h) n}{2} + \frac{\sinh(k_p H_s)}{2 \sinh(4\Lambda)} \left[1 + f_1(\tilde{\nabla}h) n \right] + \frac{1}{2} \left(\frac{\pi \varepsilon \mathfrak{G}}{4}\right)^2 \left\{ \tilde{\chi}_1 + \chi_1 \left[1 + \frac{\sinh(k_p H_s)}{\sinh(4\Lambda)} \right] \left[1 + f_1(\tilde{\nabla}h) n \right] \right\} \quad . \quad (32)$$

We carry the calculation of the non-homogeneous Γ to

leading order in $\tilde{\nabla}h$ as depicted in figure 8, correcting

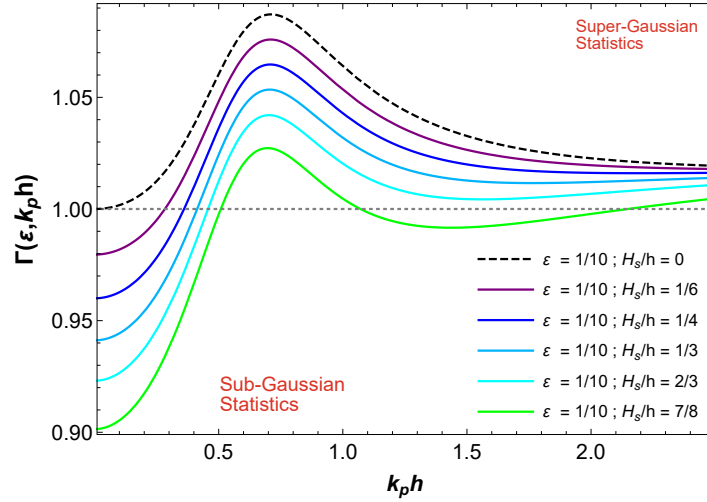


FIG. 8: Effect of breaking proxy ratio H_s/h on the non-homogeneous parameter defining anomalous wave statistics according to the approximation of eq. (34). The dashed line depicts the theoretical curve for small-amplitude waves of Mendes *et al.* [49].

Mendes and Kasparian [25] to account for finite amplitude waves (note that at the peak amplification $\Lambda \sim 1/2$

we have $n \sim 3/4$, thus $f_1(\tilde{\nabla}h)n \sim -\tilde{\nabla}h/4$):

$$\Gamma \approx \frac{1 + \frac{\pi^2 \varepsilon^2 \mathfrak{S}^2}{16} \tilde{\chi}_1}{1 - \frac{\tilde{\nabla}h}{8} + \frac{\sinh(k_p H_s)}{2 \sinh(4k_p h)} \left[1 - \frac{\tilde{\nabla}h}{4} \right] + \frac{\pi^2 \varepsilon^2 \mathfrak{S}^2}{32} \left(\tilde{\chi}_1 + \left[1 + \frac{\sinh(k_p H_s)}{\sinh(4k_p h)} \right] \left[1 - \frac{\tilde{\nabla}h}{4} \right] \chi_1 \right) + \tilde{\mathcal{E}}_{p2}}, \quad (33)$$

where $\tilde{\mathcal{E}}_{p2}$ is the net potential energy due to the change in mean water level along the shoal, being approximated as $(5\varepsilon^2/\Lambda^2)\tilde{\nabla}h(1 + \tilde{\nabla}h) \lesssim \tilde{\nabla}h/5$. At this regime of maximum amplification of statistics, we clearly see that $\tilde{\mathcal{E}}_{p2} - \frac{\tilde{\nabla}h}{8} \approx 0$. Furthermore, the typical value of $n_{2\varepsilon}/n_\varepsilon$ at the regime of interest in intermediate waters that we otherwise assumed to be equal to unity for simplicity is of $7/8$, which will weaken both terms $1 - \frac{\tilde{\nabla}h}{4}$. In fact, the effect of $1 - \tilde{\nabla}h/4 \lesssim 1.05$ adjusted by $n_{2\varepsilon}/n_\varepsilon$ is even smaller for wave trains traveling from deep water towards shallow water. Hence, we can further approximate eq. (33) in the steep slope regime where the slope effect saturates:

$$\Gamma \approx \frac{1 + \frac{\pi^2 \varepsilon^2 \mathfrak{S}^2}{16} \tilde{\chi}_1}{1 + \frac{\sinh(k_p H_s)}{2 \sinh(4k_p h)} + \frac{\pi^2 \varepsilon^2 \mathfrak{S}^2}{32} \left(\tilde{\chi}_1 + \left[1 + \frac{\sinh(k_p H_s)}{\sinh(4k_p h)} \right] \chi_1 \right)}. \quad (34)$$

Note that there is no favored steepness measure between (ε, ϵ) , and we keep them together, so the role of H_s/h is visible in the limit of $k_p h \rightarrow 0$. Clearly, the denominator has increased in magnitude, whereas the numerator has not changed in comparison with the result of Section 3 of Mendes *et al.* [49]. Thus, we expect a significant decrease in Γ towards a weaker deviation from a Gaussian sea extreme wave statistics, even to the point of a sub-Gaussian behavior near wave-breaking conditions

as depicted in figure 8. If, however, waves are traveling over a slope starting already in shallow water, then $1 - \tilde{\nabla}h/4 \lesssim 2$ and the approximation of eq. (34) overestimates Γ in breaking conditions. Nonetheless, this has no qualitative impact on the trend of the wave statistics. Indeed, the approximation for waves starting the evolution in deep water already shows that in shallow water we achieve strong sub-Gaussian statistics. Therefore, if the evolution already starts in shallow water this sub-Gaussian statistics will be stronger.

C. Excess Kurtosis

Recently, Mendes and Kasparian [26] have shown how to estimate the excess in the kurtosis of the sea surface elevation directly from Γ :

$$\mu_4 = \frac{1}{9} \left[e^{8(1 - \frac{1}{\mathfrak{S}^2 \Gamma})} - 1 \right] \approx \frac{1}{9} \left[e^{8(1 - \Gamma^{-1 - \kappa})} - 1 \right], \quad (35)$$

where $\kappa = \ln \mathfrak{S}(\varepsilon, \Lambda) / \ln \Gamma(\varepsilon, \Lambda)$ is an asymmetry parameter introduced to better meet initial conditions prior to the shoal ($\mu_4 \approx 0$), see Section 3.4 of Mendes *et al.* [49]. According to appendix B of Mendes and Kasparian [26], we may approximate $\mathfrak{S} \approx (7/6)(1 + 2\varepsilon)$. Thus, we compute κ through eq. (34) and display its features in figure

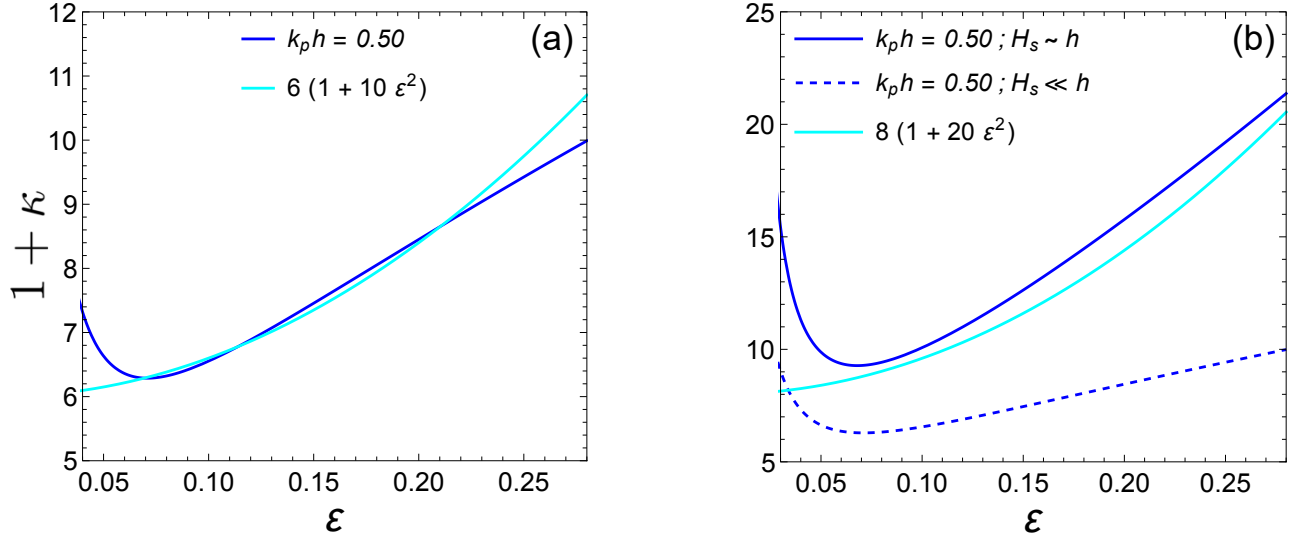


FIG. 9: Asymmetry parameter κ as a function of steepness and wave breaking proxy H_s/h . Blue lines depict the exact calculation, whereas cyan curves show polynomial approximations.

9. One can observe (figure 9a) that for small-amplitude waves of second-order in steepness ($0.05 \lesssim \varepsilon \lesssim 0.10$) the approximation $1 + \kappa = 6$ is reasonable, hence used elsewhere in a more specific context [62]. However, figure 9b demonstrates that this is no longer the case if waves are of finite amplitude and near wave breaking conditions, and now $1 + \kappa \gtrsim 10$. The latter happens because while the asymmetry has increased with steepness as expected [63] and the wave field portrays a sawtooth pattern along the breakwater (see figure 4), the kinetic energy strongly exceeds the potential energy with larger ratios H_s/h , thus, decreasing Γ . Noteworthy, the differences between ki-

netic and potential energies are well-known for progressive nonlinear waves, yet no consequences for extreme wave statistics have previously been drawn [64–67].

The exponential form for the excess kurtosis is evidently very burdensome given the complexity of eq. (34) and that $1 + \kappa \sim 6(1 + \mathcal{O}(\varepsilon^2))$. Following the steps of Section 2.2 of Zhang *et al.* [62], we attempt to perform a Taylor expansion in ε around 0 on eq. (35). Denoting $\varepsilon \equiv k_p H_s \approx (\pi/\sqrt{2})\varepsilon$, the first Taylor expansion is performed on eq. (34), leading to a finite-amplitude correction to eq. (2.16) of Zhang *et al.* [62]:

$$\Gamma_\varepsilon \approx 1 + \frac{\varepsilon^2}{\Lambda^2} - \frac{\sinh \varepsilon}{2 \sinh(4\Lambda)} \left(1 + \frac{4\varepsilon^2}{3\Lambda^6}\right) \approx 1 + \left(\frac{\varepsilon}{\Lambda}\right)^2 - \frac{\sinh \varepsilon}{2 \sinh(4\Lambda)} \left[1 + 20 \left(\frac{\varepsilon}{\Lambda}\right)^2\right]. \quad (36)$$

The second step requires us to expand the power $\Gamma^{1+\kappa} \approx 1 + (1 + \kappa)(\Gamma - 1)$ since $\Gamma - 1 \ll 1$. Thus, the main part

of the exponential calculation boils down to $1 - \Gamma^{-1-\kappa} \approx 1 + [1 + (1 + \kappa)(\Gamma - 1)]^{-1} \approx 1 - [1 - (1 + \kappa)(\Gamma - 1)] \approx (1 + \kappa)(\Gamma - 1)$. Wherefore, we achieve,

$$\begin{aligned} \mu_4 &\approx \frac{1}{9} \left[e^{8(1+\kappa)(\Gamma-1)} - 1 \right] \approx \frac{1}{9} \left[1 + 8(1+\kappa)(\Gamma-1) + \frac{64}{2!} (1+\kappa)^2 (\Gamma-1)^2 - 1 \right], \\ &\approx \frac{(1+\kappa)}{9} \left[8(\Gamma-1) + 32(1+\kappa)(\Gamma-1)^2 \right]. \end{aligned} \quad (37)$$

On the other hand, while figure 10 shows that in the region of highest amplification of extreme waves ($k_p H_s \gtrsim 1/2$) the sub-Gaussian behavior will not be present (fig-

ure 10). In contrast, the expansion of eq. (37) is not heavy tailed at $k_p H_s \gtrsim 0.3$. In other words, it is challenging for eq. (36) to sustain a numerical equivalency with

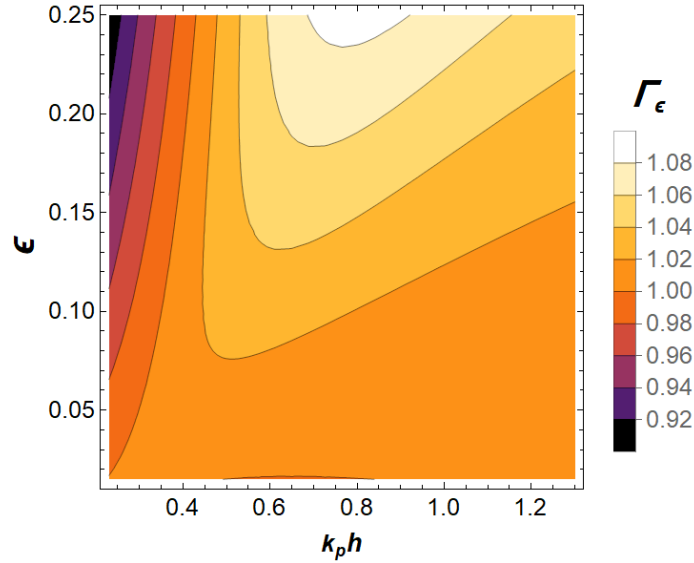


FIG. 10: Evolution of the non-homogeneous parameter with relative water depth.

the full model in the upper steepness range. Of course,

applying eq. (36) into eq. (37) allows one to expect the formula,

$$\mu_4 \approx \frac{(1 + \kappa)}{9} \left[8 \left(\frac{\epsilon}{\Lambda} \right)^2 + 32(1 + \kappa) \left(\frac{\epsilon}{\Lambda} \right)^4 - \frac{\sinh \epsilon}{\sinh(4\Lambda)} \left(1 + 200 \left(\frac{\epsilon}{\Lambda} \right)^2 \right) \right]. \quad (38)$$

No matter how much refinement is pursued analytically, the expansion can not portray the upper steepness range. This is partly due to the term $(1 + \kappa)$. Thus, although a obtaining a polynomial approximation is difficult, we

may use the best semi-analytical expression arising from this mathematical structure numerically fitted to the behavior of the full model:

$$\mu_4 \approx 8 \left(\frac{\epsilon}{\Lambda} \right)^2 + 32 \left(\frac{\epsilon}{\Lambda} \right)^4 \cdot \left(\frac{1 + \epsilon}{12\epsilon^2} \right) - \frac{\sinh \epsilon}{\sinh(4\Lambda)} \left[1 + 200 \left(\frac{\epsilon}{\Lambda} \right)^2 - 40 \left(\frac{\epsilon}{\Lambda} \right)^8 \right], \quad \Lambda > 0.5. \quad (39)$$

Note that the expression $(1 + \epsilon)/12\epsilon^2$ arises from computing $1 + \kappa$ from eq. (36) for small-amplitude waves instead of the full model of eq. (34) and is compensated by the positive term $(40 \sinh \epsilon / \sinh(4\Lambda))(\epsilon/\Lambda)^8$ that better captures the heavy tail of the curve. The fact that the modification to the analytical expansion is calculated through κ suggests that whatever part of the accuracy of the approximation was lost in the Taylor expansion could be recovered by the latter.

In addition to simplifying the main calculation for the kurtosis, these consecutive Taylor expansions help understanding the roots for the peak in kurtosis and its saturation/decay thereof. For instance, the first term $8(\epsilon/\Lambda)^2$ accounts for the effect of bound harmonics on the ex-

ceedance probability and is the leading term for weakly nonlinear seas. It is not at all surprising that its order in steepness is the same across computations of deep water regimes following the Zakharov equation [48] and other shoaling frameworks [20, 68]. The second term of this expansion is proportional to ϵ^4 . It arises from the fact that now we are no longer in weakly nonlinear seas but rather in the realm of higher-order theories in steepness. As one would expect, for one additional order in steepness the kurtosis responds with the square of that, and thus the fourth power is expected. Interestingly, the integral properties bring forth the next order despite the need to reformulate the surface elevation, thus providing the sought effective theory. Finally, the term with hy-

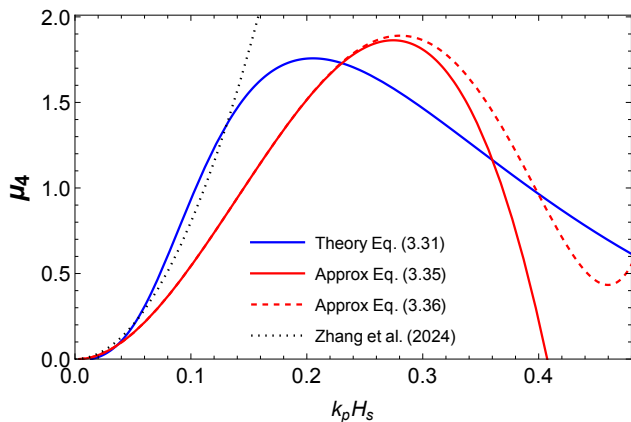


FIG. 11: Growth and saturation of the excess kurtosis of irregular waves fields traveling from deep water up to $k_p h = 1/2$ atop a breakwater. The peak of kurtosis is reached when $H_s \approx h/2$ and slowly decays onwards.

perbolic trigonometric functions describes how the finite amplitude waves affect not only the bound harmonics (polynomials) but also the kinetic energy. The novelty and rather unusual shape of this term in the context of statistical hydrodynamics likely relies on the fact that a unified description of integral properties up to wave breaking had not been attempted so far.

As seen in figure 11, the approximation for the full model does accomplish its goals. First and foremost, the kurtosis grows quickly as a function of $\mathcal{O}(\epsilon^2)$ at a given relative water depth as expected from the small-amplitude formula [62] for arbitrary slopes. The latter model has $\mu_4 = 20\pi^2(\epsilon/\Lambda)^2\sqrt{\nabla h}$ up to steep slopes tamping reflection, whose slope effect stems from the drop in potential energy density due to the set-down along the shoal [69].

The rapid growth of kurtosis along steep slopes is consistent with bound-harmonics effects as described in Li *et al.* [20] or Mori and Janssen [48]. Secondly, the kurtosis reaches its peak between $0.5 < H_s/h < 0.6$ as wave-breaking occurrence starts and the excess in kinetic energy dominates the bound harmonics. Note that in the context of shoaling, this constitutes an unexplored regime with no prior theoretical description. Finally, the kurtosis decays because the term $200(\epsilon/\Lambda)^2 \sinh \epsilon / \sinh(4\Lambda)$ strongly compensates the leading-order solution of Zhang *et al.* [62], that is, the waves must break due to high values of H_s/h in addition to being very steep. Nevertheless, as pointed out in Zhang *et al.* [62], these consecutive Taylor expansions preclude the approximations of eqs. (38, 39) to provide a good spatial evolution of kurtosis, but rather serve to estimate the maximum kurtosis atop the shoal or at its end.

More importantly, in figure 12 we compare the experimental results with the theory for the excess kurtosis, that is, plugging eq. (34) into eq. (35). We also compare with the semi-analytical approximation of eq. (39).

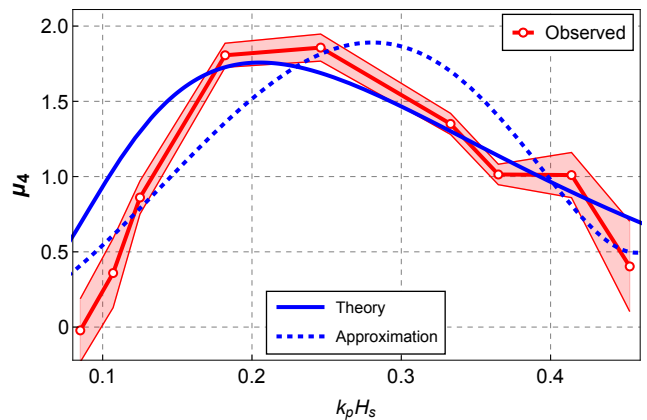


FIG. 12: Comparison between experimental, (derived) theoretical and Taylor-expanded approximated maximum excess kurtosis atop the shoal. The shaded areas correspond to the 95% confidence intervals.

Both theoretical formulations overpredict the kurtosis for steepness $k_p H_s \lesssim 0.1$, which can be related to the omission of the effect of reflection in the theory [32]. This is consistent with the empirical formulation for reflection $K_R \approx 0.1\xi^2$ over sloping beaches [70], in which ξ denotes the surf similarity and is computed in terms of the bottom slope and mean steepness $\xi \sim \nabla h / \sqrt{\epsilon}$ [29]. Wave regimes with the smallest wave steepness will therefore have the most underestimated reflection rates and thus, overestimate the kurtosis. For the bulk of second-order steepness, both models describe the laboratory results well until its peak, whereas the heavy tail for conditions nearing wave breaking is also captured well. Consequently, we validate the theoretical expectations about the time and reason of the kurtosis growth saturation and decay.

The importance of our theoretical result is the following: second-order models for rogue wave statistics since Tayfun [71] expect in a way or another the relentless growth of kurtosis with an ever-increasing steepness. As pointed out in Mendes *et al.* [21], this creates a boundless exceedance probability and consequently a boundless kurtosis. However, wave steepness can not grow boundlessly [72, 73]. Our formulae describe when and why the kurtosis growth saturates, and how fast it decays in the transition from the bound-harmonics phase leading to super-Gaussian statistics [14, 16, 20] to the wave-breaking phase featuring sub-Gaussian statistics [34, 35, 74].

IV. CONCLUSION

In this work, we have experimentally investigated statistical properties of irregular long-crested waves traveling over a symmetrical and steep breakwater in intermediate water. We have characterized and quantified how the breakwater amplifies the excess kurtosis of the

surface elevation and increases rogue wave occurrence. Our results cover up to the regime where incident waves are so steep that they resort to the finite wave amplitude theory. When the significant wave height is small compared to the water depth atop the shoal, the excess kurtosis of the surface elevation quickly grows. However, as waves become steeper, two different types of wave breaking emerge, growing slowly from just a few waves until full dominance. A continuous variation between the two cases shows that beyond a threshold of $k_{p2}H_s \sim 0.25$, and wave breaking balances the effect of steepness, thus decreasing the excess kurtosis and the rogue wave occurrence. We compute this significant wave height threshold from the developed theory and find good agreement with experiments. We therefore unify the picture for rogue wave amplification due to shoaling over wide ranges of relative water depth, steepness, and height-to-depth ratio based on experimental evidence and theoretical developments. Our results contrast to previous ones over flat bottoms up to the breaking limit or based on the Glukhovskiy distribution, which in the surf zone ($k_p h \lesssim 0.5$) describes the decrease of the excess kurtosis to negative (sub-Gaussian) values in the wave breaking regime.

We compute second-order corrections due to the height-to-depth ratio based on a finite amplitude theory for the spectral kinetic energy up to the second order in steepness. Combining this correction with previous knowledge on the potential energy, we obtain a theoretical description of the experiments carried out in a wave flume: when waves are of second-order but small steepness $k_{p2}H_s \lesssim 0.2$, the variance of the surface elevation increases at a faster rate than the total spectral energy, for a given water depth atop the shoal. Hence the steepness drives the intensification of a non-Gaussian behavior. On the other hand, as soon as some waves break, even in minimal proportion, the picture is inverted and the total spectral energy grows faster than the variance. Hence, we are able to unify the statistical behavior of irregular long-crested waves across all water depth regimes even in the presence of different levels of energy dissipation and wave breaking.

This combined theoretical and experimental study confirms the possibility of treating irregular waves as second-order even if they belong to a regime of high-orders in steepness, or to an even more complex solution such as cnoidal waves. We therefore unify non-homogeneous processes from a purely stochastic viewpoint. Thus, we overcome the classical challenge of unifying water wave equations and solutions. Thus, we demonstrate that stochastic analysis of irregular water waves does not consist of a simple and yet cumbersome study of collections of regular waves. Rather, we hint at the existence of fundamental principles of stochastic wave analysis that can not be transferred to the deterministic counterpart.

From a statistical point of view, early wave breaking is generally expected to decrease the probability of rogue wave breakers. However, we have shown that the this probability increases if the beach slope is sufficiently steep to tamp reflection. Since rogue wave breakers feature the highest loads on ships or marine structures, and therefore are the most hazardous, this hazard is highest over steep slopes. Therefore, breakwaters should be conceived with slopes below $\sim 1/5$ in zones prone to very steep sea conditions.

V. ACKNOWLEDGEMENTS

S.M. and J.K. were supported by the Swiss National Science Foundation under grant 200020-175697. Y.H. acknowledges the support from the Distinguished Postdoctoral Fellowship Scheme of the Hong Kong Polytechnic University. A.C. acknowledges support from Okinawa Institute of Science and Technology (OIST) with subsidy funding from the Government of Japan's Cabinet Office. Authors are also grateful to Dr. Kapil Chauhan and Theo Gresley-Daines from the University of Sydney for their support and advice on the experimental setup and valuable help with the installation.

Declaration of Interests. The authors report no conflict of interest.

-
- [1] P. Liu, A chronology of freak wave encounters, *Geofizika* **24**, 57 (2007).
 - [2] S. Haver, A possible freak wave event measured at the draupner jacket january 1 1995, *Proc. Rogue Waves 20-22 October IFREMER* (2004).
 - [3] D. Faulkner and W. Buckley, Critical survival conditions for ship design, *International Conference on Design and Operation for Abnormal Conditions, RINA* **6**, 1 (1997).
 - [4] D. Faukner, Shipping safety: A matter of concern, *Ingenia, The Royal Academy of Engineering, Marine Matters*, 13 (2002).
 - [5] E. Bitner-Gregersen and O. Gramstad, Rogue waves: Impact on ships and offshore structures, *DNV GL Strategic Research & Innovation Position Paper* (2015).
 - [6] T. Tang, D. Barratt, H. B. Bingham, T. S. van den Bremer, and T. A. A. Adcock, The impact of removing the high-frequency spectral tail on rogue wave statistics, *Journal of Fluid Mechanics* **953**, A9 (2022).
 - [7] Z. Li, T. Tang, Y. Li, S. Draycott, T. S. van den Bremer, and T. A. A. Adcock, Wave loads on ocean infrastructure increase as a result of waves passing over abrupt depth transitions, *Journal of Ocean Engineering and Marine Energy* **9**, 309 (2023).
 - [8] Z. Xin, X. Li, and Y. Li, Coupled effects of wave and depth-dependent current interaction on loads on a bottom-fixed vertical slender cylinder, *Coastal Engineer-*

- ing **183**, 104304 (2023).
- [9] Y. Li and A. Chabchoub, On the formation of coastal extreme waves in water of variable depth, *Cambridge Prisms: Coastal Futures* **1**, e33 (2023).
- [10] K. Trulsen, H. Zeng, and O. Gramstad, Laboratory evidence of freak waves provoked by non-uniform bathymetry, *Phys. Fluids* **24** (2012).
- [11] H. Kashima and N. Mori, Aftereffect of high-order non-linearity on extreme wave occurrence from deep to intermediate water, *Coastal Engineering* **153**, 103559 (2019).
- [12] J. Zhang, M. Benoit, O. Kimmoun, A. Chabchoub, and H.-C. Hsu, Statistics of extreme waves in coastal waters: Large scale experiments and advanced numerical simulations, *Fluids* **4** (2019).
- [13] Y. Zheng, Z. Lin, Y. Li, T. Adcock, Y. Li, and T. Van Den Bremer, Fully nonlinear simulations of unidirectional extreme waves provoked by strong depth transitions: The effect of slope, *Phys. Rev. Fluids* **5** (2020).
- [14] K. Trulsen, A. Raustøl, S. Jorde, and L. Rye, Extreme wave statistics of long-crested irregular waves over a shoal, *J. Fluid Mech.* **882** (2020).
- [15] Y. Li, S. Draycott, T. A. Adcock, and T. Van Den Bremer, Surface wavepackets subject to an abrupt depth change. part 2: Experimental analysis, *J. Fluid Mech.* **915**, A72 (2021).
- [16] J. Zhang and M. Benoit, Wave-bottom interaction and extreme wave statistics due to shoaling and de-shoaling of irregular long-crested wave trains over steep seabed changes, *Journal of Fluid Mechanics* **912**, A28 (2021).
- [17] O. Kimmoun, H.-C. Hsu, N. Hoffmann, and A. Chabchoub, Experiments on uni-directional and nonlinear wave group shoaling, *Ocean Dynamics* (2021).
- [18] J. Zhang, Y. Ma, T. Tan, G. Dong, and M. Benoit, Enhanced extreme wave statistics of irregular waves due to accelerating following current over a submerged bar, *J. Fluid Mech.* **954**, A50 (2023).
- [19] C. Bolles, K. Speer, and M. Moore, Anomalous wave statistics induced by abrupt depth change, *Physical Review Fluids* **4** (2019).
- [20] Y. Li, S. Draycott, Y. Zheng, Z. Lin, T. Adcock, and T. Van Den Bremer, Why rogue waves occur atop abrupt depth transitions, *Journal of Fluid Mechanics* **919**, R5 (2021).
- [21] S. Mendes, A. Scotti, and P. Stansell, On the physical constraints for the exceeding probability of deep water rogue waves, *Appl. Ocean Res.* **108**, 102402 (2021).
- [22] A. Raustøl, *Freaker bølger over variabelt dyp*, Master's thesis, University of Oslo (2014).
- [23] B. Le Méhauté, *An introduction to hydrodynamics and water waves*, Springer (1976).
- [24] C. Lawrence, K. Trulsen, and O. Gramstad, Statistical properties of wave kinematics in long-crested irregular waves propagating over non-uniform bathymetry, *Physics of Fluids* **33** (2021).
- [25] S. Mendes and J. Kasparian, Saturation of rogue wave amplification over steep shoals, *Phys. Rev. E* **106**, 065101 (2022).
- [26] S. Mendes and J. Kasparian, Non-homogeneous kurtosis evolution of shoaling rogue waves, *J. Fluid Mech.* **966**, A42 (2023).
- [27] V. Katsardi, L. de Lutio, and C. Swan, An experimental study of large waves in intermediate and shallow water depths. part i: Wave height and crest height statistics, *Coastal Eng.* **73**, 43 (2013).
- [28] R. Fu, Y. Ma, G. Dong, and M. Perlin, A wavelet-based wave group detector and predictor of extreme events over unidirectional sloping bathymetry, *Ocean Eng.* **229** (2021).
- [29] L. H. Holthuijsen, *Waves in Oceanic and Coastal Waters* (Cambridge University Press, 2007).
- [30] S. Hallowell, A. T. Myers, and S. R. Arwade, Variability of breaking wave characteristics and impact loads on offshore wind turbines supported by monopiles, *Wind Energy* **19**, 301–312 (2015).
- [31] A. Toffoli, D. Proment, H. Salman, J. Monbaliu, F. Frascoli, M. Dafilis, E. Stramignoni, R. Forza, M. Manfrin, and M. Onorato, Wind generated rogue waves in an annular wave flume, *Physical Review Letters* **118** (2017).
- [32] Y. He, *Experiments on nonlinear extreme waves in complex configurations*, Doctoral thesis, The University of Sydney (2023).
- [33] Y. He, T. Kanehira, N. Mori, M. Gamaleldin, A. Babanin, K. Chauhan, and A. Chabchoub, Nonlinear and extreme wave group interactions with a circular cylinder, *Proc. Int. Conf. Offshore Mech. Arct. Engng - OMAE*, 104739 (2023).
- [34] J. Xu, S. Liu, J. Li, and W. Jia, Experimental study of wave height, crest, and trough distributions of directional irregular waves on a slope, *Ocean Engineering* **242**, 110136 (2021).
- [35] I. Karpadakis, C. Swan, and M. Christou, A new wave height distribution for intermediate and shallow water depths, *Coastal Engineering* **175**, 104130 (2022).
- [36] P. Bonneton, Energy and dissipation spectra of waves propagating in the inner surf zone, *Journal of Fluid Mechanics* **977**, A48 (2023).
- [37] N. J. Zabusky and M. D. Kruskal, Interaction of "solitons" in a collisionless plasma and the recurrence of initial states, *Physical review letters* **15**, 240 (1965).
- [38] S. Trillo, G. Deng, G. Biondini, M. Klein, G. Clauss, A. Chabchoub, and M. Onorato, Experimental observation and theoretical description of multisoliton fission in shallow water, *Physical review letters* **117**, 144102 (2016).
- [39] M. Longuet-Higgins, On the statistical distribution of the heights of sea waves, *Journal of Marine Research* **11**, 245 (1952).
- [40] S. Rice, Mathematical analysis of random noise, *Bell Syst. Tech. J.* **23**, 282 (1944).
- [41] P. Boccotti, Some new results on statistical properties of wind waves, *Applied Ocean Research* **5**, 134 (1983).
- [42] H. Cramér, *Studies in the history of probability and statistics. xxviii. on the history of certain expansions used in mathematical statistics*, *Biometrika* **59**, 205 (1972).
- [43] S. M. S. Mendes, On the statistics of oceanic rogue waves in finite depth: Exceeding probabilities, physical constraints and extreme value theory, UNC Chapel Hill PhD Thesis. (2020).
- [44] M. Longuet-Higgins, The effect of non-linearities on statistical distributions in the theory of sea waves, *J. Fluid Mech.* **17**, 459 (1963).
- [45] F. Y. Edgeworth, The generalised law of error, or law of great numbers, *Journal of the Royal Statistical Society* **69**, 497 (1906).
- [46] T. Marthinsen, On the statistics of irregular second-order waves, Report No. RMS-11 (1992).
- [47] N. Mori and T. Yasuda, A weakly non-gaussian model of wave height distribution random wave train, *Ocean Eng.*

- 29**, 1219–1231 (2002).
- [48] N. Mori and P. Janssen, On kurtosis and occurrence probability of freak waves, *J. Phys. Oceanogr.* **36**, 1471 (2006).
- [49] S. Mendes, A. Scotti, M. Brunetti, and J. Kasparian, Non-homogeneous model of rogue wave probability evolution over a shoal, *J. Fluid Mech.* **939**, A25 (2022).
- [50] A. Babanin, *Breaking and Dissipation of Ocean Surface Waves* (Cambridge University Press, 2011).
- [51] W. Mostert and L. Deike, Inertial energy dissipation in shallow-water breaking waves, *Journal of Fluid Mechanics* **890**, A12 (2020).
- [52] I. Karmpadakis and C. Swan, On the average shape of the largest waves in finite water depths, *Journal of Physical Oceanography* **50**, 1023 (2020).
- [53] Y. Kim, N. Kalligeris, T.-J. Hsu, and P. J. Lynett, Large eddy simulation study of a wave-induced shallow-water monopolar vortex, *Ocean Modelling* **162**, 101796 (2021).
- [54] S. Liu, H. Wang, A.-C. Bayeul-Lainé, C. Li, J. Katz, and O. Coutier-Delgosha, Wave statistics and energy dissipation of shallow-water breaking waves in a tank with a level bottom, *Journal of Fluid Mechanics* **975**, A25 (2023).
- [55] M. Antuono, Steady periodic waves over a planar seabed: a global characterization, *Journal of Fluid Mechanics* **947**, A18 (2022).
- [56] K. Zhao, Y. Wang, and P. L.-F. Liu, A guide for selecting periodic water wave theories-le méhauté (1976)’s graph revisited, *Coastal Engineering* **188**, 104432 (2024).
- [57] Y. Iwagaki, Hyperbolic waves and their shoaling, *Coastal Engineering in Japan* **11**, 1 (1968).
- [58] Y. Iwagaki, K. Shiota, and H. Doi, Shoaling and refraction coefficient of finite amplitude waves., *Coastal Engineering in Japan* **25**, 25 (1982).
- [59] M. Isobe, Calculation and application of first-order cnoidal wave theory, *Coastal engineering* **9**, 309 (1985).
- [60] R. Dean and R. Dalrymple, *Water wave mechanics for engineers and scientists.*, World Scientific (1984).
- [61] C. C. Mei, M. A. Stiassnie, and D. K.-P. Yue, *Theory and applications of ocean surface waves: Part 2: Nonlinear aspects* (World Scientific, 2005).
- [62] J. Zhang, S. Mendes, M. Benoit, and J. Kasparian, Effect of shoaling length on rogue wave occurrence, *Journal of Fluid Mechanics* (2024).
- [63] M. A. Tayfun and M. A. Alkhalidi, Distribution of sea-surface elevations in intermediate and shallow water depths, *Coastal Eng.* **157** (2020).
- [64] V. P. Starr, Momentum and energy integrals for gravity waves of finite height, *Journal of Marine Research* 6(3): 175-193 (1947).
- [65] G. W. Platzman, The partition of energy in periodic irrotational waves of the surface of deep water, *Journal of Marine Research* 6(3): 194-202 (1947).
- [66] L. R. Mack and B. E. Jay, The partition of energy in standing gravity waves of finite amplitude, *Journal of Geophysical Research* **72**, 573 (1967).
- [67] M. S. Longuet-Higgins, Integral properties of periodic gravity waves of finite amplitude, *Proceedings of the Royal Society of London. A. Mathematical and Physical Sciences* **342**, 157 (1975).
- [68] T. Yasuda and N. Mori, Occurrence properties of giant freak waves in sea area around japan, *J. Waterway, Port, Coastal Ocean Eng.* **123**, 209 (1997).
- [69] S. Mendes and J. Kasparian, Slope effect on the evolution of kurtosis over a shoal, *ASME 42nd International Conference on Ocean, Offshore & Arctic Engineering - OMAE2023* (2023).
- [70] J. Battjes, Surf similarity, *Coastal Engineering Proceedings* **1**, 26 (1974).
- [71] M. A. Tayfun, Narrow-band nonlinear sea waves, *J. Geophys. Res.* **85**, 1548 (1980).
- [72] G. Stokes, On the theory of oscillatory waves, *Trans. Camb. Phil. Soc.* **8**, 441–455 (1847).
- [73] R. Miche, Mouvements ondulatoires de la mer en profondeur constante ou décroissante forme limite de la houle lors de son deferlement, *Ann. Ponts Chaussees* **121**, 285–319 (1944).
- [74] B. Glukhovskii, Investigation of sea wind waves (in russian), *Gidrometeoizdat* (1966).